Effects of quantum nuclear delocalisation on NMR parameters from path integral molecular dynamics

Martin Dračínský,*[a,b] Paul Hodgkinson*[a]

[a] Dr. Martin Dračínský, Dr. Paul Hodgkinson, Department of Chemistry, Durham University, South Road, DH1 3LE, Durham, UK
Fax: (+44) 191-394-4737
E-mail: dracinsky@uochb.cas.cz, paul.hodgkinson@durham.ac.uk
[b] Institute of Organic Chemistry and Biochemistry, Flemingovo nám. 2, 16610, Prague, Czech Republic

Key words: density functional calculations, NMR spectroscopy, nuclear delocalisation, isotope effects, path integral molecular dynamics

Abstract

The influence of nuclear delocalisation on NMR chemical shifts in molecular organic solids is explored using path integral molecular dynamics (PIMD) and density functional theory calculations of shielding tensors. Nuclear quantum effects are shown to explain previously observed systematic deviations in correlations between calculated and experimental chemical shifts, with particularly large PIMD-induced changes (up to 23 ppm) observed for atoms in methyl groups. The PIMD approach also enables isotope substitution effects on chemical shifts and *J* couplings to be predicted in excellent agreement with experiment for both isolated molecules and molecular crystals. An approach based on convoluting calculated shielding or coupling surfaces with probability distributions of selected bond distances and valence angles obtained from PIMD simulations is used to calculate isotope effects.

Introduction

The gauge-including projector-augmented wave (GIPAW) procedure has been recently developed for the prediction of the magnetic resonance parameters in solids,[1] and the power of this approach for calculating NMR properties for fully periodic crystal structures has been well documented.[2] Such quantum chemical calculations are typically performed using static structures, i.e. at 0 K. It is well established, however, that fast molecular motions, such as vibrations, conformational averaging, and molecular aggregation, will average NMR parameters.[2a, 3] In particular, rovibrational averaging of shielding is observed as isotope shifts.[4] Neglecting zero-point motion and dynamics may lead to significant discrepancies between computed and experimental data.

Plots of calculated ^{13}C shielding values against experimental chemical shifts generally show slopes that deviate from the ideal value of –1. This complicates the referencing of the calculated shielding values and typically linear regression between calculated and experimentally determined values is used to improve agreement.[5] This makes the comparison of chemical shifts obtained in different studies difficult because the fitted parameters vary between experimental data sets , with the fitted slope, usually between –1 and –1.2[2b, 6], being heavily dependent on the type of molecule. For example, trendlines with slopes of –1.05 and –1.16 respectively, have been found for aromatic vs. carbohydrate shielding values. Such systematic deviations may limit the ability to use shielding

calculations for spectral assignments.[7] This behaviour has variously been attributed to errors intrinsic to approximations of DFT,[8] but also the effects of molecular motion.[9]

Classical and *ab initio* molecular dynamics methods have been widely applied to study the influence of molecular motion on NMR parameters; see for example ref.[2a, 3, 10] However, nuclear quantum effects, such as zero-point vibrations and tunnelling, may be crucial in the case of light nuclei, particularly hydrogen atoms. A comparison of vibrational averaging at zero temperature and finite temperature has revealed a significant contribution of zero-point motion to calculated chemical shifts.[4, 9, 11] The quantum vibrational phenomena might not be sufficiently characterized even by *ab initio* dynamics that uses Newtonian mechanics for the nuclei (classical nucleus MD). One route to including quantum effects on nuclear motion is provided by the formalisms based on Feynman's path integral[12] (PI) approach. Path integral simulations use a decomposition of nuclei into a number of beads subject to specific harmonic nearest neighbour interactions. The strength of the harmonic interaction depends on nuclear mass and temperature, with light nuclei at low temperature being highly delocalised (see Figure S1 in SI for a schematic representation). The ensemble of coordinates for a given set of beads, termed a replica, is propagated in time, forming a path integral trajectory. Static properties of quantum objects can thus be obtained by simulating more complicated, but still classical, objects using well-established simulation techniques such as molecular dynamics or Monte Carlo simulations.[13] The underlying potential energy landscape may be expressed within classical force-fields or any *ab initio* methods.[14]

The path integral approach has been employed in a wide variety of applications.[15] In the context of NMR, PIMD has been used with classical force-field potentials for a protein fragment[16] and liquid water simulation.[17] PIMD used with *ab initio* methods was applied in a study of isolated deprotonated water dimer ($H_3O_2^-$), and showed significant differences in the delocalisation of the hydrogen-bonded vs. non-hydrogen-bonded protons at different temperatures.[18] Path integral Monte Carlo simulations with *ab initio* methods have been used to determine the influence of nuclear fluctuations on chemical shifts of isolated bullvalene,[19] ethylene,[20] and benzene.[21] Changes of carbon chemical shifts of several ppm were observed. Path integrals with Car-Parrinello molecular dynamics were used to predict ^{1}H NMR chemical shifts in solid $LiNH_2$ and Li_2NH. Almost no effect of nuclear quantum delocalisation was found for Li_2NH whereas a broader distribution of ^{1}H chemical shifts in $LiNH_2$ was found when path integration was applied.[22] We are not, however, aware of previous systematic investigations of the effects of nuclear delocalisation on NMR spectra of organic solids.

Isotope effects are one manifestation of the quantum nature of nuclei; zero-point fluctuations lead to differences in vibrationally averaged properties of compounds with isotopic substitution. Isotope effects in NMR have a multitude of practical applications, such as in the determination of molecular structure and the verification of mechanisms of reactions. The small size of isotope effects, however, makes them stringent tests of *ab initio* calculations.[23] A conventional route to calculating isotope shifts involves calculation of intramolecular force field and shielding surface (the dependence of isotropic shielding on nuclear coordinates). However, this procedure is computationally demanding and is suitable only for small isolated molecules.[4] For larger molecules and molecular crystals, many approximations (such as a drastic reduction of molecular degrees of freedom) have to be employed.[24]

Here we use a combination of PIMD with DFT to explore the influence of nuclear quantum effects on the NMR isotropic shielding of organic molecular solids and to predict deuterium isotope effects on chemical shifts and coupling constants. We demonstrate that nuclear delocalisation

(particularly of hydrogen atoms) has a significant impact on bond distances and ^{13}C chemical shifts. The PIMD approach is also used for predictions of deuterium substitution effects on chemical shifts and *J* couplings.

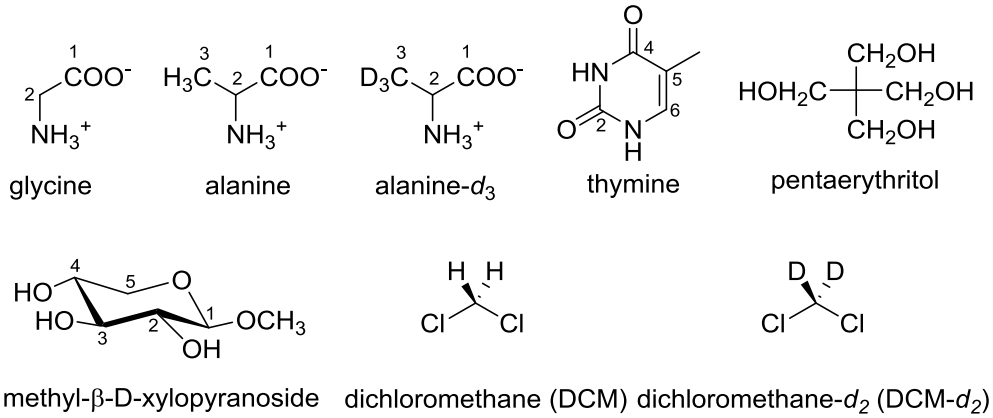

Figure 1. The studied model compounds with atom numbering.

Methods

Samples of alanine, alanine-d_3, and thymine were obtained from Sigma Aldrich. High-resolution solid-state NMR spectra were obtained using a Varian/Chemagnetics InfinityPlus spectrometer operating at 125.7 MHz for ^{13}C (499.7 MHz for ^{1}H). Samples were packed into 5 mm magic angle spinning rotors and measurements taken using a MAS rate of 10 kHz using cross polarisation (CP). The typical CP conditions used were: recycle delay 4 s, contact time 2 ms, acquisition time 40 ms. Spectra were referenced with respect to external neat tetramethylsilane for ^{13}C by setting the high-frequency signal from a replacement sample of adamantane to 38.5 ppm. A correction of +16 K was made to the set temperatures to correct for the frictional heating of the sample under sample spinning.

Figure 1 shows the set of model compounds used for the calculations. The atomic coordinates for glycine (GLYCIN20), alanine (LALNIN12), methyl-β-D-xylopyranoside (XYLOBM01), pentaerythritol (PERYTO10), and thymine (THYMIN01) were obtained from the Cambridge Crystallographic Database.[25] For glycine, alanine, the xylopyranoside, and pentaerythritol, neutron diffraction structures were used. Neutron data were unavailable in the case of thymine, and X-ray structures were used. Note that for consistency all crystal structures used were determined at room temperature.

Born-Oppenheimer molecular dynamics (BOMD) simulations were run in the CASTEP program,[26] which is a DFT-based code, using an *NVT* ensemble maintained at a constant temperature of 300 K using a Langevin thermostat, a 0.5 fs integration time step, ultrasoft pseudopotentials,[27] a planewave cutoff energy of 300 eV, and with integrals taken over the Brillouin zone using a Monkhorst-Pack[28] grid of a minimum k-point sampling of 0.1 $Å^{-1}$. Electron-correlation effects were modeled using the generalized gradient approximation of Perdew, Burke, and Ernzerhof.[29] The atomic positions were optimized at the same computational level prior to the MD runs, while lattice parameters were fixed to the experimental values. No symmetry constraints were applied during the runs as these are only relevant to the time-averaged structure. Simulation runs of 5 ps were performed for every compound. Dichloromethane was modeled as an isolated molecule in

a cubic periodic box of 11 x 11 x 11 $Å^3$, and was pre-equilibrated by 5 ps (PI)MD simulations to equilibrate the random initial partition of the kinetic energy into rotations, translations and vibrations. The path integral was used on top of the DFT-MD simulations, with a Trotter decomposition of all nuclei into P = 16 beads.

Time-averaged NMR parameters were computed from 41 snapshots from the MD and PIMD simulations selected at 1.0, 1.1, 1.2 … 5.0 ps. The unit cells of glycine, alanine and thymine contained four crystallographically equivalent molecules (Z = 4); Z = 2 for the xylopyranoside and pentaerythritol unit cells; therefore, 164 or 82 values were averaged for every chemically equivalent site. The standard deviations of the calculated shieldings for chemically equivalent sites were used for an estimation of the error of the calculation. The real time snapshots from the PIMD simulations contained 16 replicas and the NMR tensors calculated for the individual replicas were averaged. The NMR calculations were performed using the GIPAW approach,[1, 30] using 'on-the-fly' pseudopotentials, a planewave cutoff energy of 600 eV with integrals taken over the Brillouin zone using a Monkhorst-Pack[28] grid of a minimum k-point sampling of 0.05 $Å^{-1}$.

A reasonable convergence of the calculated isotropic shieldings (changes typically less than 1 ppm for ^{13}C) was usually achieved after the averaging of 20–30 real-time snapshots. The convergence of the isotropic shielding of atom C3 in alanine is illustrated in Figure S2 in the SI. This convergence is much faster than when calculating NMR parameters of compounds in solution, where the rapid fluctuation of the solvent molecules requires the averaging of several hundreds or thousands MD snapshots to obtain reasonably converged chemical shifts.[31]

The (PI)MD-induced change of isotropic shielding was then calculated as the difference between the averaged NMR parameters and those calculated on a ''(PI)MD-averaged structure'' structure where the positions of all atoms during the (PI)MD simulation were averaged. As discussed previously,[10] atomic motion means that the average distance between atoms is not the same as the distance between averaged atomic positions, and such an MD-averaged structure is more directly comparable with the diffraction structures obtained at the same temperature. Calculating the (PI)MD-induced change in this way, as opposed to relative to 0 K geometry-optimised structure, also avoids any systematic errors introduced by imperfect geometry optimisation. Where required for comparison with experimental data, NMR parameters were calculated as the values computed from the diffraction structure plus the (PI)MD-induced change (referred to as CSD + (PI)MD data), i.e. σ_{iso} = σ_{iso}(static) + $\Delta\sigma_{iso}$. Alternatively, the averaged PIMD shieldings were compared directly with experimental shifts. PIMD simulation of alanine with P = 32 decomposition gave calculated PIMD-induced changes of chemical shifts were close to those calculated with P = 16 (maximum differences were 0.32 and 0.08 ppm, for ^{13}C and ^{1}H respectively).

The following procedure was used to calculate deuterium isotope effects on alanine. Probability distributions of the C3–H bond distance and C2–C3–H valence angle (alanine), and of the C–H bond distance and H–C–H valence angle (dichloromethane) were extracted from the (PI)MD simulations. The PIMD distance/angle probabilities were determined independently for all 16 replicas and then averaged. Then a dependence of isotropic shieldings in alanine on the bond distance and the valence angle was calculated by manually adjusting the C3–H bond distance in the range 0.9–1.4 Å (with a 0.05 Å step) and a C2–C3–H valence angle ranging from 80° to 140° (5° step). The calculated dependence of the shielding values on the geometrical parameters was fitted to a polynomial function (order 2 for the distance and 3 for the angle dependence). The probability distributions and the polynomial functions were then used to calculate weighted averages of shielding values of alanine and alanine-d_3 and for the chemical shift changes induced by the isotope

substitution. This approach of 1D scans through the shielding surface, rather than a full, but very computationally expensive, 2D parameterisation, is appropriate if the effects of the distance and angle on nuclear shielding are largely additive. We checked the additivity by calculating the carbon shielding dependence on the methyl C–H distance for three different C2–C3–H angles (100, 110, and 120°) and the calculated dependences were very similar (differences lower than 10%. A similar procedure was applied for dichloromethane, where the dependence of carbon shielding values and $^{1}J_{C\text{-}H}$ coupling constants on the C–H distance and H–C–H angle of isolated dichloromethane was calculated using B3LYP functional[32] and 6-31g** basis set with the Gaussian09 program.[33] The *J* coupling was calculated in the range 0.7–2.0 Å (with a 0.05 Å step) and 70°–150° (5° step). The carbon shielding dependence fitted well to a quadratic curve whereas the *J* coupling dependence had a more complicated form, and so *J* coupling values as a function of distance were calculated by linear extrapolation between neighbouring calculated points. The isotope effect on *J*-coupling is calculated as the difference $J_{C\text{-}H}(\text{DCM}) - {}^{*}J_{C\text{-}H}(\text{DCM-}d_2)$, where ${}^{*}J_{C\text{-}H}(\text{DCM-}d_2) = J_{C\text{-}D}(\text{DCM-}d_2) \times \gamma_H/\gamma_D$.

Results

Effects on isotropic shieldings

Figure 2 shows the probability distributions of the methyl C–H bond distance and of the C2–C3–H angle in alanine and in alanine-d_3 observed during MD and PIMD simulations. As expected, the atoms, especially hydrogens, are more delocalised in the PIMD simulations. The PIMD distributions are also shifted slightly towards longer bond lengths. The scatter of nuclear positions of hydrogen H2 in alanine during MD and PIMD simulations is shown in Figure S3 in SI.

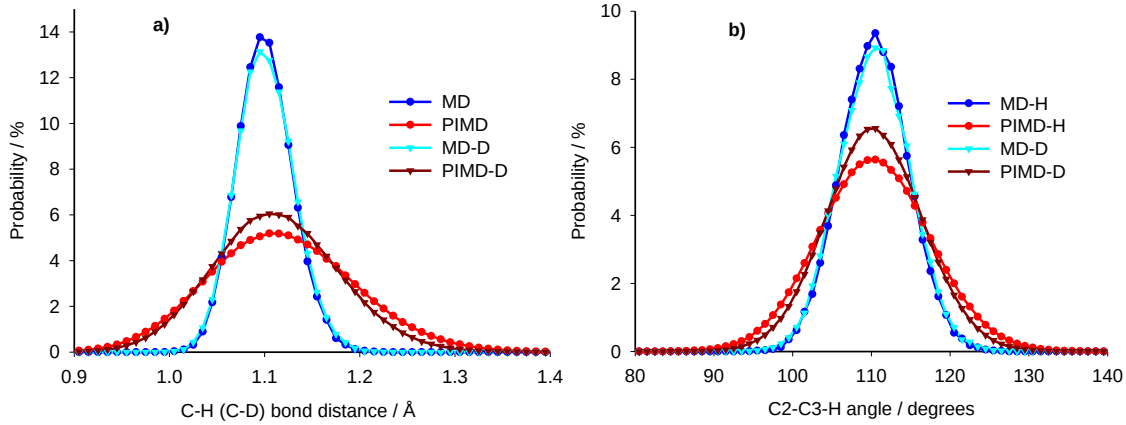

Figure 2. Probability distribution of C–H/C–D bond distances in the methyl group (a) and of C2–C3–H angle (b) of alanine during the MD and PIMD simulations at 300 K, sampled by 0.01 Å and 1° respectively.

The calculated PIMD-induced changes of shielding values were negative for all atoms, i.e. the atoms are less shielded when the nuclear motion is taken into account. This presumably reflects the shift in the probability distribution towards longer bond lengths, reducing the shielding effect of the electrons at the nuclei. The PIMD-induced changes for the ^{13}C shielding were found in the range 3.3–22.5 ppm (see Table S1 in SI) with the magnitude roughly correlating with the number of attached hydrogen atoms. The changes were particularly large, and quite variable, for methyl carbons (Figure 3): alanine 9.2 ppm, xylopyranoside 18.6 ppm, and thymine 22.5 ppm. The corrections seem to correlate with the degree of delocalisation of the CH_3 hydrogens (see Figure 3b).

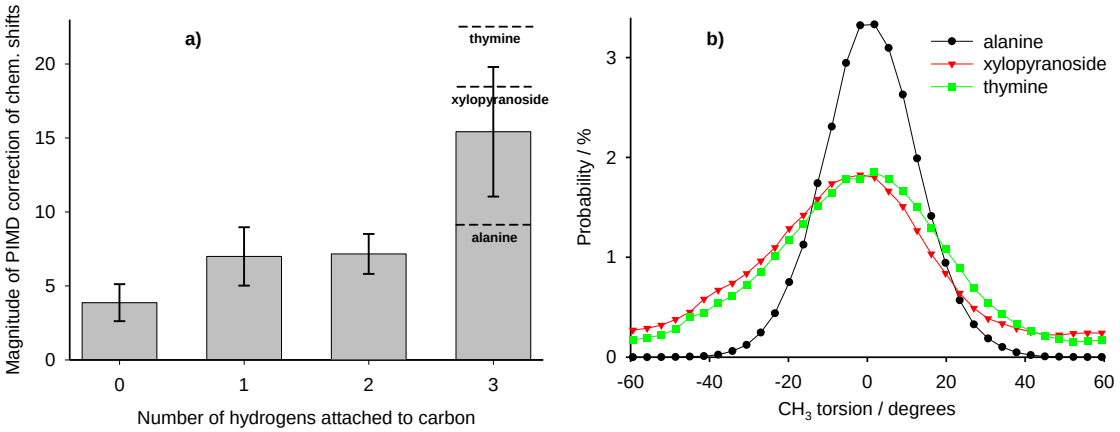

Figure 3. (a) Dependence of the calculated PIMD-induced changes of carbon chemical shifts on number of attached hydrogen atoms. Dashed lines indicate individual PIMD-induced shifts for methyl groups. (b) Probability distribution of CH_3 torsions in alanine, xylopyranoside and thymine relative to equilibrium geometry.

The inclusion of the PIMD corrections leads to a very good agreement between experimental and calculated chemical shift differences in the individual structures. For example, the $\delta_{C1} - \delta_{C3}$ difference in alanine is predicted to be 157.4 ± 0.9 ppm, which is very close to the experimental value (see Table 1), while the values calculated for the diffraction structure and for the geometry optimized structure is 163.1 and 168.0 ppm respectively. Figure 4 depicts the correlation between the experimental ^{13}C chemical shifts of all crystalline samples in this study and the isotropic shielding values calculated with and without the PIMD correction. The fitting line for the static calculations (without PIMD) has a slope of –1.055, which is a typical value found for organic molecular crystals. Geometry optimization of all atomic positions does not improve the slope considerably (–1.046, see Table 2) and neither does including MD-induced changes (slope –1.048). On the other hand, when the PIMD corrections are included, the shielding-shift correlation fits to a straight line with slope –0.992 ± 0.015, i.e. –1 within the scatter of the points. The RMSD of the linear fit with PIMD corrections is 3.1 ppm, which is better than for the starting CSD structures (4.9 ppm) but worse than for geometry-optimised structures (1.9 ppm). The improvement of the shielding-shift correlation after adding the PIMD corrections to the calculations using the CSD structures suggests that the deviations between the CSD-based shieldings and experimental shifts is largely due to the effects of molecular motion on the average structure observed by diffraction. When the averaged PIMD shieldings are compared directly with experimental shifts (without calculating the PIMD-induced shift and adding it to the CSD values), the RMSD of the linear fit is only slightly worse.

The marginally poorer overall fit of the PIMD results in comparison to the geometry-optimised structure is initially surprising given the improvement in the overall degree of correlation. However, the differences between PIMD-induced changes calculated for otherwise equivalent asymmetric units within the unit cell (corresponding to the average estimated error of 0.95 ppm) strongly suggest this difference is largely the result of imperfect convergence. In the limit of a very large number of snapshots, the residuals for the PIMD-corrected results are likely to be as least as small as those determined using the single geometry-optimised structure. This convergence is, however, relatively slow, cf. Figure S2 in the SI.

Table 1. ^{13}C experimental chemical shifts (ppm) and calculated isotropic shieldings (ppm) of alanine.

Method	C1	C2	C3	δ(C1) – δ(C3)
Calculated σ, CSD	–6.54	122.10	156.60	163.14
Calculated σ, geom. opt	–16.11	120.60	151.85	167.96
Calculated σ, CSD + MD	–9.80 ± 0.34	119.35 ± 0.72	150.52 ± 1.16	160.32 ± 1.21
Calculated σ, CSD + PIMD	–10.02 ± 0.13	116.69 ± 0.41	147.37 ± 0.93	157.39 ± 0.94
Experimental δ	177.76	50.94	20.39	157.37

Table 2. Parameters of linear fitting obtained for calculated shielding vs. experimental shift correlations of all studied crystalline samples, RMSD between fitted and experimental points, and average estimated errors (AEE) of the (PI)MD-induced shifts.

Method	Slope	Intercept / ppm	RMSD / ppm	AEE / ppm
CSD	–1.055 ± 0.024	178.59 ± 2.47	4.9	-
Geom. opt.	–1.046 ± 0.009	172.1 ± 0.97	1.9	-
CSD + MD	–1.048 ± 0.024	174.8 ± 2.46	4.9	0.79
CSD + PIMD	–0.992 ± 0.015	165.16 ± 0.94	3.1	0.95
PIMD	–1.012 ± 0.016	163.00 ± 1.63	3.2	0.95

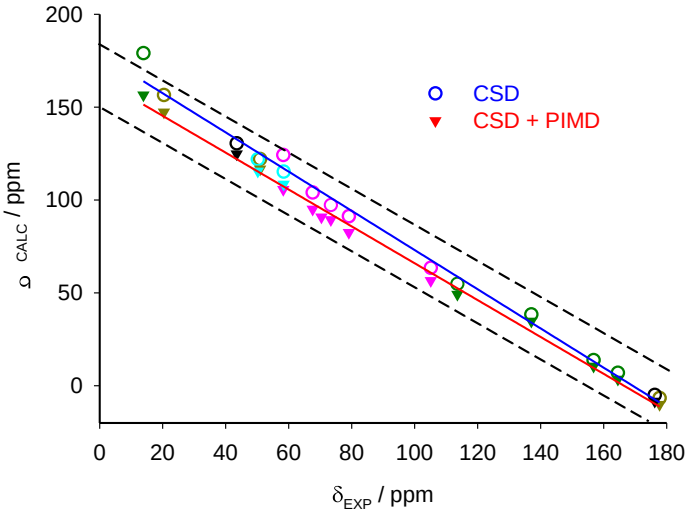

Figure 4. The correlation between calculated shielding values and experimental chemical shifts of glycine (black), alanine (dark yellow), thymine (green), pentaerythritol (cyan), and methyl-β-D-xylopyranoside (pink). The calculations were done for diffraction structures with (triangles) and without (empty circles) PIMD induced changes. The black dashed lines with the expected slope of –1 show the systematic deviation of the slope of the CSD fit (blue) compared to the CSD + PIMD slope (red). The linear fitting parameters are summarised in Table 2. The experimental chemical shifts of methyl-β-D-xylopyranoside and pentaerythritol are from refs.[34] and,[35] respectively.

The PIMD induced shifts of hydrogen atoms were found in the range 0.2–2.8 ppm (see Table S2 in the SI). Similar to the trends observed for carbon, the largest PIMD-induced shifts were found for hydrogen atoms in methyl groups and, again, the order of the magnitude of the methyl group

PIMD-induced shifts was thymine > xylopyranoside > alanine i.e. correlated to the degree of angular delocalisation. The lack of experimental data (currently only for glycine and alanine) limits further general conclusions.

Calculation of deuterium isotope effects

The experimental effects of deuterium substitution on ^{13}C shielding, which can be measured to within approximately 0.05 ppm, are shown in Figure 5 and tabulated in Table 3. The estimated errors of the snapshot-based shielding calculation are too high for a prediction of such small effects, as can be seen in Table 3, where the error of the calculations based on the snapshot approach is of the same order as the isotope effect. Therefore, we used a different approach for the prediction of the isotope effects. The most important geometrical factors are expected to be the change in C–H bond distance and C2–C3–H valence angle distributions upon isotope substitution.[24a] We calculated the dependence of the isotropic shieldings of alanine on the methyl C–H bond distance and the C2–C3–H valence angle (Figure 6) and used the bond distance and valence angle probabilities obtained from the MD and PIMD simulations (Figure 2) to determine weighted averages of the ^{13}C isotropic shieldings. This approach is computationally much less demanding than the method of snapshot calculations, where 656 NMR calculations are necessary for 41 snapshots from PIMD trajectory with P = 16. This approach resembles previous attempts to predict isotope effects by calculating 1D potential and shielding dependences for selected stretching vibrations.[24] However, the probability distributions obtained from PIMD simulations incorporate contributions from all possible molecular motions to the selected bond distance or valence angle. It can be seen in Table 3 that the deuterium isotope effect calculations based on the PIMD bond distributions are all in excellent agreement with the experimental values. On the other hand, the MD-based values completely fail to reproduce the experimental data.

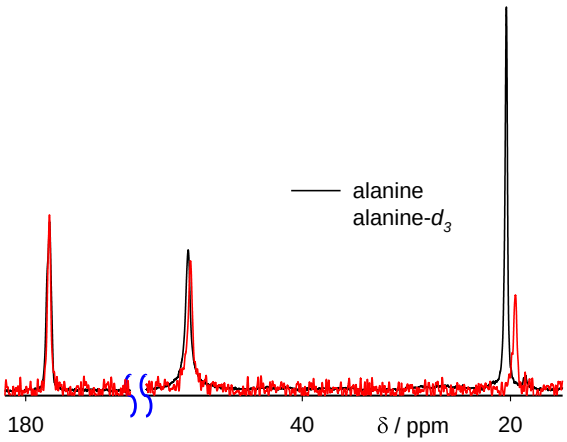

Figure 5. Experimental ^{13}C spectra of alanine (black) and alanine-d_3 (red). Note the break on the chemical shift axis between 55 and 170 ppm.

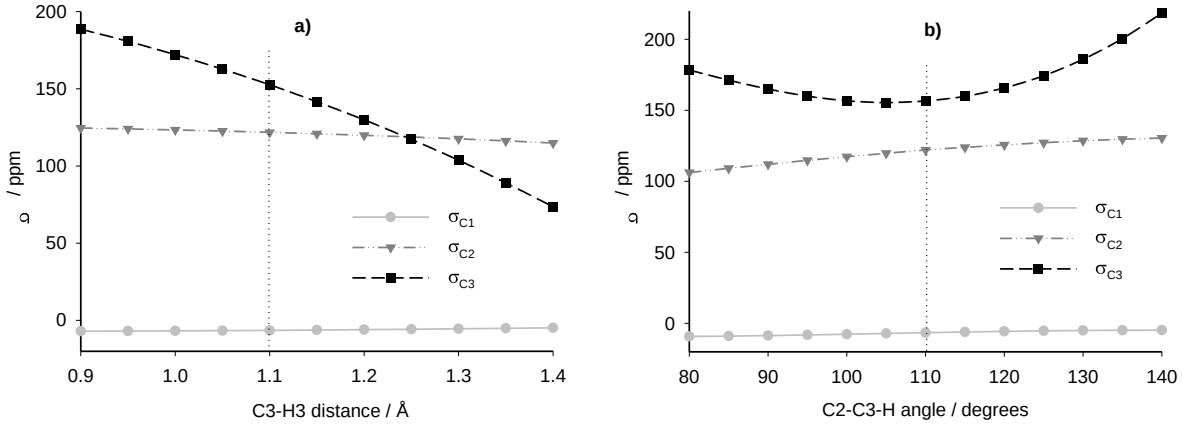

Figure 6. The calculated dependence of ^{13}C isotropic shieldings on the methyl C-H bond distance (a) and the C2-C3-H valence angle (b) in alanine. The vertical dotted lines represent the equilibrium values. The polynomial fitting parameters are summarised in Table S3 in the SI.

Table 3. Calculated and experimental effects of C3 (methyl) deuterium isotope substitution on the ^{13}C chemical shifts of alanine (ppm). Calculated data obtained by averaging shielding values for the MD/PIMD snapshots (columns MD-snap and PIMD-snap) or by convoluting the methyl C–H bond distance and C2–C3–H angle probability distributions by the dependence of calculated shieldings on the distance and the angle (columns MD-prob and PIMD-prob).

		δH – δD				
		MD-snap	MD-prob	PIMD-snap	PIMD-prob	Exptl.
C1	C3–H3 distance		0.00		–0.04	
	C2–C3–H3 angle		0.00		0.00	
	Total	0.04 ± 0.80	0.00	–0.26 ± 1.15	–0.04	–0.05
C2	C3–H3 distance		–0.01		0.13	
	C2–C3–H3 angle		0.00		0.05	
	Total	0.23 ± 1.25	–0.01	0.79 ± 0.69	0.18	0.20
C3	C3–H3 distance		–0.09		1.53	
	C2–C3–H3 angle		0.07		–0.60	
	total	–0.21 ± 0.96	–0.02	1.63 ± 0.93	0.93	0.85

To further investigate the potential of the PIMD approach for the prediction of changes of NMR parameters induced by isotope substitution, we calculate the deuterium isotope effect on carbon chemical shift and C-H *J* coupling in dichloromethane. The calculated dichloromethane deuterium isotope effects were compared with reported experimental solution-state data.[36] The experimental isotope effect was shown to be almost solvent and concentration independent implying that intermolecular interactions may be omitted in the isotope effect calculations. The most important geometrical factors are expected to be the change in C–H bond distance and H–C–H valence angle distributions upon isotope substitution.[24a] These probability distributions obtained in the (PI)MD simulations are shown in Figure S4 in the SI. The PIMD distributions are again much broader than the MD ones.

We calculated the dependence of the carbon shielding and the $J_{C\text{-}H}$ coupling on the C–H bond distance and the H–C–H angle over the range of distances and angles found in the PIMD simulations as described in the Methods section (see Figure S5 in the SI). The averaged NMR parameters were determined by convolution of the bond distance distributions obtained from PIMD with the distance dependence of the shift and coupling. Table 4 shows that the deuterium isotope effect calculations based on the PIMD probability distributions are very close to the experimental values for both the carbon chemical shift and the *J* coupling.

Table 4. Experimental[36a, 36b] and calculated deuterium isotope effects on carbon chemical shifts and indirect $^1J_{CH}$ coupling in dichloromethane.

		Calculated-PIMD	Experimental
$^{13}C(CH_2Cl_2) - {}^{13}C(CD_2Cl_2)$ / ppm	C–H distance	0.23	
	H–C–H angle	0.21	
	Total	0.44	0.40
$J_{CH}(CH_2Cl_2) - J_{CH}(CD_2Cl_2)$ / Hz	C–H distance	0.12	
	H–C–H angle	0.58	
	Total	0.70	0.86 ± 0.06

Conclusions

We have demonstrated that quantum nuclear effects have a significant influence on NMR chemical shifts. The nuclear delocalisation leads to broad distributions of bond distances, particularly those of light hydrogen nuclei. This delocalisation causes deshielding of the attached atoms, with the magnitude of the effect roughly correlating with the number of attached hydrogens, with particularly large effects for methyl groups. Since methyl resonances are clustered in the low-frequency region of ^{13}C spectra and the high-frequency region is dominated by non-protonated carbons such as carbonyls, this may explain why shielding-shift correlations typically deviate from the expected slope of –1 and why this deviation is essentially eliminated when nuclear delocalisation effects are included. It may be significant that large slope deviations (–1.16) have been reported for carbohydrate derivatives containing multiple methyl groups, while the trendline for the aromatic compounds (without any methyl groups) had a slope of –1.05.[7]

Both the classical nucleus and path integral MD add an uncertainty to the averaged shielding values related to the convergence of the data with respect to the number of snapshots. This uncertainty is likely to explain the slightly worse RMSD found in the PIMD shielding-shift correlation when compared with calculations based on geometry-optimised structures. However, the RMSD is improved for PIMD relative to MD, and we may expect that an increase of the number of PIMD snapshots will lead to lower uncertainties and further improved correlations. On the other hand, the fact that eliminating the systematic discrepancies between calculated and experimental results does not reduce the "local" discrepancies shows that calculating NMR shieldings of a single geometry-optimised at zero kelvin does a remarkably good job of predicted experimental shifts measured at ambient temperature despite the complete neglect of molecular dynamics. A significant factor behind the success of geometry optimisation is seen to be correcting for the distorting effects of thermal motions on averaged atomic positions as measured by Bragg diffraction at finite temperatures. These observations help to retrospectively validate current approaches in "NMR

crystallography" and explain their success. In contrast, similar comparison of calculated and experimental infrared or Raman spectra of organic crystals is much less satisfactory and the use of vibrational spectroscopy for crystal structure determination is, therefore, limited.[37]

The PIMD approach enables predictions of isotope effects in larger systems such as organic molecular crystals in excellent agreement with experiment. Convergence errors, which would otherwise dominate the calculated results, can be avoided by convoluting probability distributions of selected geometrical parameters with the calculated shielding or *J* coupling surface scans. This approach provides insight into the geometrical factors contributing to the isotope effect, and is computationally much less demanding than the method of snapshot calculations.

Acknowledgement

The research leading to these results has received funding from the People Programme (Marie Curie Actions) of the European Union's Seventh Framework Programme (FP7/2007-2013) under REA grant agreement n° 299242.

References

[1] C. J. Pickard, F. Mauri, *Phys. Rev. B* **2001**, *6324*, 245101.
[2] a) C. Bonhomme, C. Gervais, F. Babonneau, C. Coelho, F. Pourpoint, T. Azais, S. E. Ashbrook, J. M. Griffin, J. R. Yates, F. Mauri, C. J. Pickard, *Chem. Rev.* **2012**, *112*, 5733-5779; b) R. K. Harris, P. Hodgkinson, C. J. Pickard, J. R. Yates, V. Zorin, *Mag. Res. Chem.* **2007**, *45*, S174-S186.
[3] A. C. De Dios, C. J. Jameson, in *Annual Reports on NMR Spectroscopy, Vol. 77* (Ed.: G. A. Webb), Elsevier Ltd., Burlington, **2012**, pp. 1-80.
[4] M. Dračínský, J. Kaminský, P. Bouř, *J. Chem. Phys.* **2009**, *130*, 094106.
[5] D. A. Forsyth, A. B. Sebag, *J. Am. Chem. Soc.* **1997**, *119*, 9483-9494.
[6] a) J. Czernek, T. Pawlak, M. J. Potrzebowski, *Chem. Phys. Lett.* **2012**, *527*, 31-35; b) J. M. Griffin, J. R. Yates, A. J. Berry, S. Wimperis, S. E. Ashbrook, *J. Am. Chem. Soc.* **2010**, *132*, 15651-15660; c) L. Truflandier, M. Paris, F. Boucher, *Phys. Rev. B* **2007**, *76*; d) R. Laskowski, P. Blaha, F. Tran, *Phys. Rev. B* **2013**, *87*; e) M. Dračínský, M. Buděšínský, B. Warzajtis, U. Rychlewska, *J. Phys. Chem. A* **2012**, *116*, 680-688.
[7] J. C. Johnston, R. J. Iuliucci, J. C. Facelli, G. Fitzgerald, K. T. Mueller, *J. Chem. Phys.* **2009**, *131*, 144503.
[8] a) M. Bühl, M. Kaupp, O. L. Malkina, V. G. Malkin, *J. Comput. Chem.* **1999**, *20*, 91-105; b) P. J. Wilson, in *Annual Rep. NMR Spectr., Vol. 49* (Ed.: G. A. Webb), Academic, New York, **2003**, pp. 117-168.
[9] J. N. Dumez, C. J. Pickard, *J. Chem. Phys.* **2009**, *130*, 104701.
[10] M. Dračínský, P. Hodgkinson, *CrystEngComm*. in press, **DOI:** 10.1039/C3CE40612A.
[11] M. Dračínský, P. Bouř, *J. Comput. Chem.* **2012**, *33*, 1080-1089.
[12] R. P. Feynman, A. R. Hibbs, *Quantum Mechanics and Path Integrals*, McGraw-Hill, New York, **1965**.
[13] A. Witt, S. D. Ivanov, M. Shiga, H. Forbert, D. Marx, *J. Chem. Phys.* **2009**, *130*, 194510.
[14] J. Zinn-Justin, *Path Integrals in Quantum Mechanics*, Oxford University Press, Oxford, **2005**.
[15] H. Kleinert, *Path integrals in quantum mechanics, statistics, and polymer physics*, World Scientific Publishing Co., Singapore, **1990**.
[16] S. Tang, D. A. Case, *J. Biomol. NMR* **2007**, *38*, 255-266.
[17] J. Lobaugh, G. A. Voth, *J. Chem. Phys.* **1997**, *106*, 2400-2410.
[18] M. Shiga, K. Suzuki, M. Tachikawa, *J. Chem. Phys.* **2010**, *132*, 114104.

[19] a) J. Schulte, R. Ramírez, M. C. Böhm, *Chem. Phys. Lett.* **2006**, *432*, 579-584; b) M. C. Böhm, R. Ramírez, J. Schulte, *Chem. Phys.* **2007**, *342*, 1-15.
[20] M. C. Böhm, J. Schulte, R. Ramírez, *Chem. Phys. Lett.* **2000**, *332*, 117-124.
[21] a) J. Schulte, R. Ramírez, M. C. Böhm, *Mol. Phys.* **2001**, *99*, 1155-1158; b) M. C. Böhm, J. Schulte, R. Ramírez, *Int. J. Quantum Chem.* **2002**, *86*, 280-296.
[22] G. A. Luduena, M. Wegner, L. Bjålie, D. Sebastiani, *ChemPhysChem* **2010**, *11*, 2353-2360.
[23] C. J. Jameson, in *Encyclopedia of NMR* (Ed.: R. K. Harris), John Wiley & Sons, Ltd, Chichester, **2012**.
[24] a) T. Dziembowska, P. E. Hansen, Z. Rozwadowski, *Prog. Nucl. Magn. Reson. Spectrosc.* **2004**, *45*, 1-29; b) J. Abildgaard, S. Bolvig, P. E. Hansen, *J. Am. Chem. Soc.* **1998**, *120*, 9063-9069.
[25] F. H. Allen, *Acta Cryst. B* **2002**, *58*, 380-388.
[26] S. J. Clark, M. D. Segall, C. J. Pickard, P. J. Hasnip, M. J. Probert, K. Refson, M. C. Payne, *Z. Kristallogr.* **2005**, *220*, 567-570.
[27] D. Vanderbilt, *Phys. Rev. B* **1990**, *41*, 7892-7895.
[28] H. J. Monkhorst, J. D. Pack, *Phys. Rev. B* **1976**, *13*, 5188-5192.
[29] J. P. Perdew, K. Burke, M. Ernzerhof, *Phys. Rev. Lett.* **1996**, *77*, 3865-3868.
[30] J. R. Yates, C. J. Pickard, F. Mauri, *Phys. Rev. B* **2007**, *76*, 024401.
[31] J. Kessler, M. Dračínský, P. Bouř, *J. Comput. Chem.* **2013**, *34*, 366-371.
[32] a) A. D. Becke, *J. Chem. Phys.* **1993**, *98*, 5648-5652; b) C. T. Lee, W. T. Yang, R. G. Parr, *Phys. Rev. B* **1988**, *37*, 785-789.
[33] M. J. Frisch, G. W. Trucks, H. B. Schlegel, G. E. Scuseria, M. A. Robb, J. R. Cheeseman, G. Scalmani, V. Barone, B. Mennucci, G. A. Petersson, H. Nakatsuji, X. Caricato, X. Li, H. P. Hratchian, A. F. Izmaylov, J. Bloino, G. Zheng, J. L. Sonnenberg, M. Hada, M. Ehara, K. Toyota, R. Fukuda, J. Hasegawa, M. Ishida, T. Nakajima, Y. Honda, O. Kitao, H. Nakai, T. Vreven, J. Montgomery, J. A., J. E. Peralta, F. Ogliaro, M. Bearpark, J. J. Heyd, E. Brothers, K. N. Kudin, V. N. Staroverov, R. Kobayashi, J. Normand, K. Raghavachari, A. Rendell, J. C. Burant, S. S. Iyengar, J. Tomasi, M. Cossi, N. Rega, J. M. Millam, M. Klene, J. E. Knox, J. B. Cross, V. Bakken, C. Adamo, J. Jaramillo, R. Gomperts, R. E. Stratmann, O. Yazyev, A. J. Austin, R. Cammi, C. Pomelli, J. W. Ochterski, R. L. Martin, K. Morokuma, V. G. Zakrzewski, G. A. Voth, P. Salvador, J. J. Dannenberg, S. Dapprich, A. D. Daniels, O. Farkas, J. B. Foresman, J. V. Ortiz, J. Cioslowski, D. J. Fox, Gaussian, Inc., Wallingford CT, **2009**.
[34] M. G. Taylor, R. H. Marchessault, S. Perez, P. J. Stephenson, C. A. Fyfe, *Can. J. Chem.* **1985**, *63*, 270-273.
[35] F. Liu, A. M. Orendt, D. W. Alderman, D. M. Grant, *J. Am. Chem. Soc.* **1997**, *119*, 8981-8984.
[36] a) N. M. Sergeyev, P. Sandor, N. D. Sergeyeva, W. T. Raynes, *J. Magn. Res. A* **1995**, *115*, 174-182; b) N. M. Sergeyev, N. D. Sergeyeva, W. T. Raynes, *J. Chem. Soc., Chem. Commun.* **1994**, 485-486; c) N. M. Sergeyev, N. D. Sergeyeva, W. T. Raynes, *Magn. Reson. Chem.* **1994**, *32*, 381-385.
[37] M. Dračínský, E. Procházková, J. Kessler, J. Šebestík, P. Matějka, P. Bouř, *J. Phys. Chem. B* **2013**, *117*, 7297-7307.

Entry for the Table of Contents

Nuclear delocalisation

Martin Dračínský, Paul Hodgkinson**
……..… Page – Page

Effects of quantum nuclear delocalisation on NMR parameters from path integral molecular dynamics

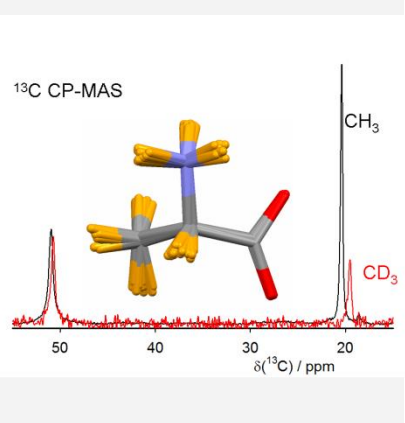

The influence of nuclear delocalisation on NMR chemical shifts is explored using path integral molecular dynamics, and is shown to explain previously observed systematic deviations between calculated and experimental shifts. PIMD also enables isotope substitution effects to be predicted in excellent agreement with experiment.

Effects of quantum nuclear delocalisation on NMR parameters from path integral molecular dynamics

Martin Dračínský,[a,b,*] Paul Hodgkinson[a,*]

[a]*Department of Chemistry, Durham University, South Road, DH1 3LE, Durham, UK*
[b]*Institute of Organic Chemistry and Biochemistry, Flemingovo nám. 2, 16610, Prague, Czech Republic*

SUPPORTING INFORMATION

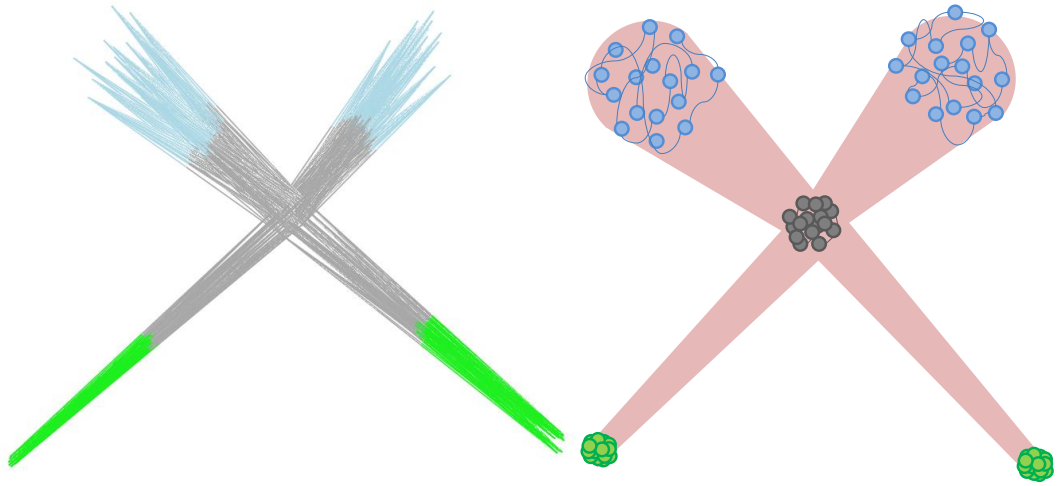

Figure S1. (Left) Randomly selected PIMD snapshot of dichloromethane using 16 replicas. (Right) Schematic representation of the decomposition of DCM into 16 replicas. Circles represent individual beads and springs represent the harmonic nearest neighbour interactions.

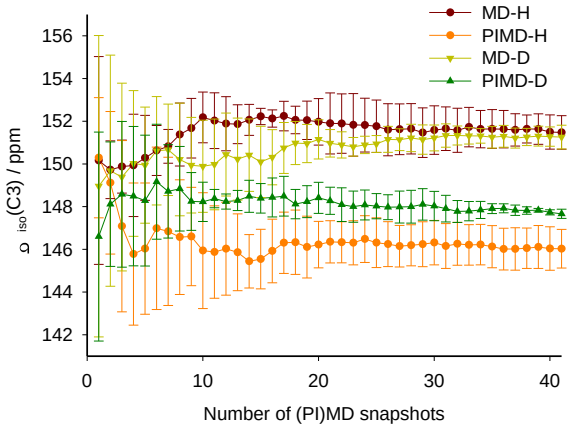

Figure S2. The convergence of the calculated isotropic shielding values of the carbon atom C3 in alanine and alanine-d_3 with respect to the number of snapshots from the MD and PIMD trajectory. The PIMD shieldings were obtained as the average of the shieldings of 16 replicas. The shielding values for the four equivalent molecules in the unit cell were averaged independently and the error bars were estimated as the standard error of this set of four values with respect to their mean.

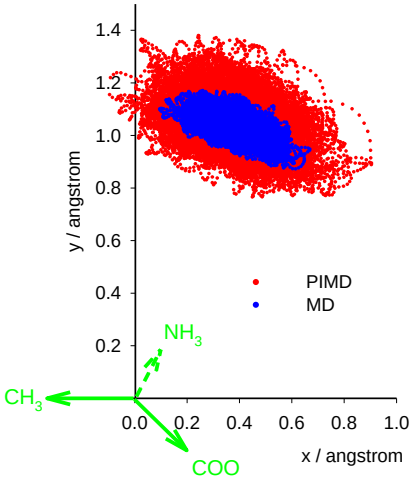

Figure S3. The scatter of hydrogen atom H2 in alanine during MD and PIMD simulations. Atom C2 is placed in the coordinate system origin, the C2–C3 bond is aligned with the –*x* axis and atoms H2, C2, and C3 lie in the *xy* plane. The blue and red dots represent the position of H2 in the course of the MD and PIMD simulations, respectively. One randomly selected bead from the PIMD simulation is shown.

Table S1. The PIMD-induced changes in ^{13}C shieldings for all the crystalline materials studied.

	Carbon	# of attached hydrogens	PIMD-induced shift
Thymine	C2	0	–3.30 ± 0.30
	C4	0	–3.49 ± 0.69
	C5	0	–5.67 ± 1.82
	C6	1	–3.65 ± 0.68
	CH_3	3	–22.52 ± 2.48
Alanine	C1	0	–3.48 ± 0.13
	C2	1	–5.41 ± 0.41
	C3	3	–9.23 ± 0.93
Xylopyranoside	C1	1	–6.87 ± 0.11
	C2	1	–7.88 ± 2.40
	C3	1	–8.76 ± 0.93
	C4	1	–9.40 ± 0.05
	C5	2	–8.98 ± 0.65
	OCH_3	3	–18.57 ± 0.13
Glycine	C1	0	–3.39 ± 0.81
	C2	2	–5.74 ± 1.08
Pentaerythrytol	C1	0	–6.39 ± 2.35
	C2	2	–6.77 ± 1.22

Table S2. The PIMD-induced changes in ^{1}H shieldings for all the crystalline materials studied.

	Hydrogen	PIMD-induced shift
Thymine	C5	–0.37
	CH_3	–2.78
	NH	–0.22, –0.32
Alanine	H2	–0.67
	CH_3	–1.18
	NH_3	–0.38
Xylopyranoside	H1	–0.86
	H2	–1.12
	H3	–1.09
	H4	–1.16
	H5	–0.91, –1.30
	OCH_3	–2.34
	OH	–1.34, –0.81, –0.60
Glycine	H2	–0.82, –0.88
	NH_3	–0.36
Pentaerythrytol	CH_2	–0.82
	OH	–0.76

Table S3. The polynomial fits of the calculated ^{13}C isotropic shieldings of alanine (in ppm) on the methyl C-H bond distance ($d_{C\text{-}H}$ / Å) and the C2-C3-H valence angle (φ / degrees). Equilibrium values of the distance and valence angle are 1.097 Å and 110.6 degrees, respectively.

$\sigma_{C1} = 5.557(d_{C\text{-}H})^2 - 8.345(d_{C\text{-}H}) - 4.006$
$\sigma_{C2} = -18.238(d_{C\text{-}H})^2 + 22.503(d_{C\text{-}H}) + 119.08$
$\sigma_{C3} = -167.81(d_{C\text{-}H})^2 + 156.79(d_{C\text{-}H}) + 183.22$
$\sigma_{C1} = -0.000033\varphi^3 + 0.0103\varphi^2 - 0.970\varphi + 19.428$
$\sigma_{C2} = -0.00405\varphi^2 + 1.301\varphi + 27.875$
$\sigma_{C3} = 0.000278\varphi^3 - 0.045\varphi^2 + 0.2385\varphi + 305.35$

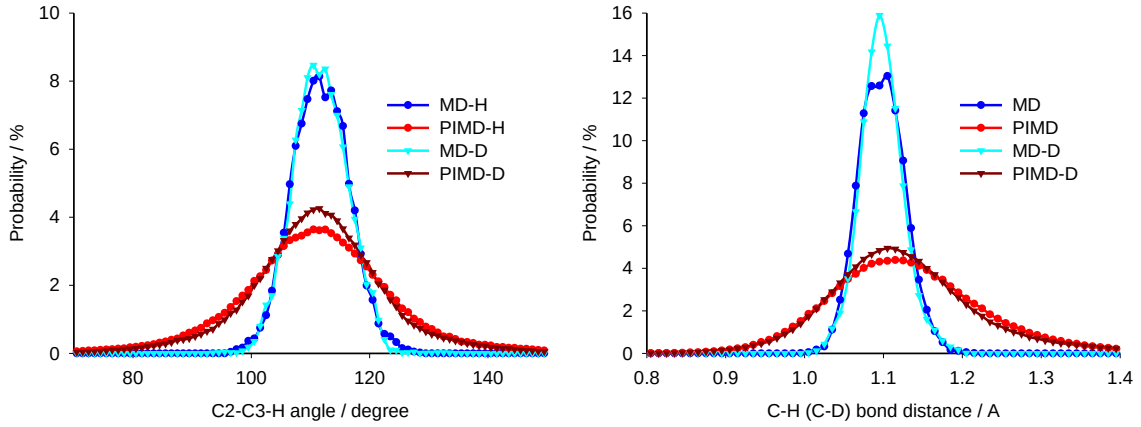

Figure S4. The probability distribution of C–H and C–D bond distances in the dichloromethane during the MD and PIMD simulations at 300 K sampled by 0.01 Å.

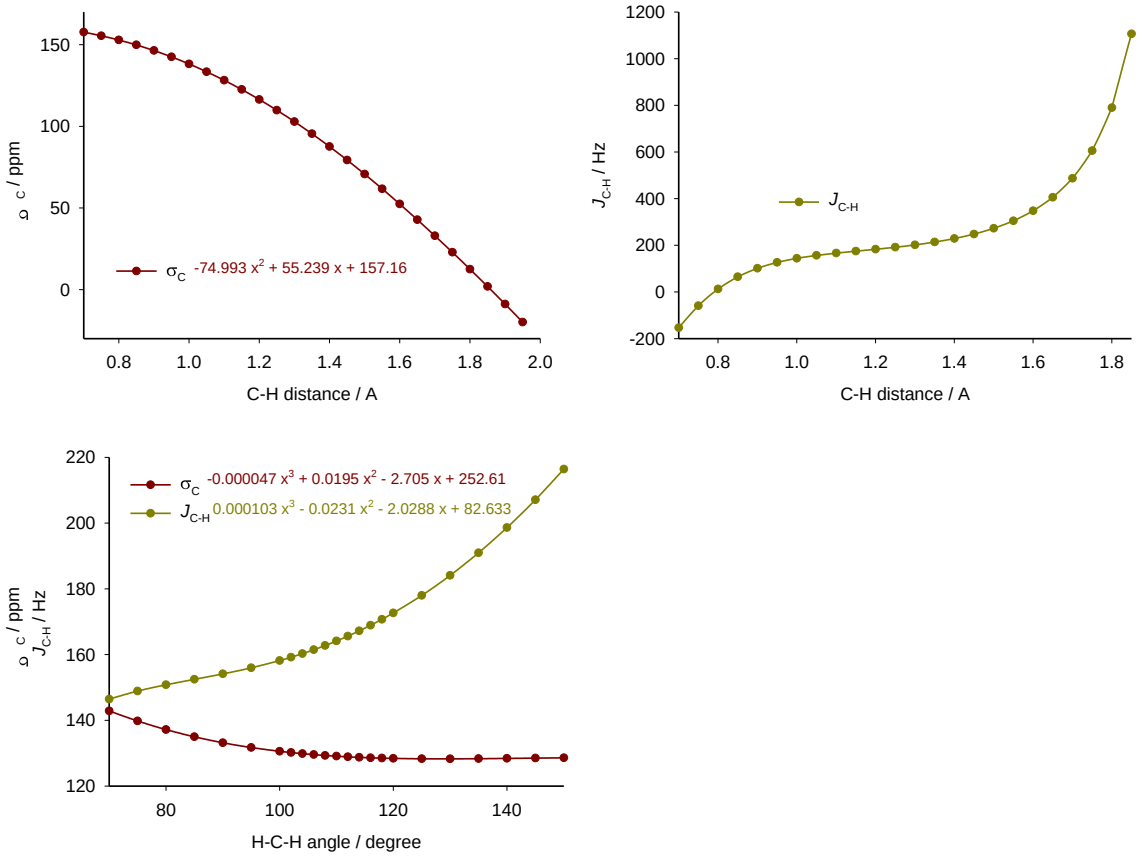

Figure S5. Calculated (B3LYP/6-31g**) dependence of ^{13}C isotropic shielding and $^{1}J_{C\text{-}H}$ coupling constant on the C-H bond distance and H-C-H valence angle in dichloromethane. Equilibrium values of the distance and valence angle are 1.093 Å and 111.4 degrees, respectively.